



Article

# Kalman–FIR Fusion Filtering for High-Dynamic Airborne Gravimetry: Implementation and Noise Suppression on the GIPS-1A System

Guanxin Wang 1,2,3, Shengqing Xiong 2,\*, Fang Yan 4,\*, Feng Luo 2, Linfei Wang 2 and Xihua Zhou 2

- School of Geophysics and Information Technology, China University of Geosciences (Beijing), Beijing 100083, China; 3010230033@email.cugb.edu.cn
- China Aero Geophysical Survey and Remote Sensing Center for Natural Resources, Beijing 100083, China; luofeng80@126.com (F.L.); wlfei4103@126.com (L.W.); xihua\_wt@163.com (X.Z.)
- <sup>3</sup> Key Laboratory of Airborne Geophysics and Remote Sensing Geology Ministry of Natural Resources, Beijing 100083, China
- Beijing Institute of Automation Control Equipment, Beijing 100074, China
- \* Correspondence: xsqagrs@126.com (S.X.); y15601390126@163.com (F.Y.)

### **Abstract**

High-dynamic airborne gravimetry faces critical challenges from platform-induced noise contamination. Conventional filtering methods exhibit inherent limitations in simultaneously achieving dynamic tracking capability and spectral fidelity. To overcome these constraints, this study proposes a Kalman-FIR fusion filtering (K-F) method, which is validated through engineering implementation on the GIPS-1A airborne gravimeter platform. The proposed framework employs a dual-stage strategy: (1) An adaptive state-space framework employing calibration coefficients  $(S_x, S_y, S_z)$  continuously estimates triaxial acceleration errors to compensate for gravity anomaly signals. This approach resolves aliasing artifacts induced by non-stationary noise while preserving low-frequency gravity components that are traditionally attenuated by conventional FIR filters. (2) A window-optimized FIR post-filter explicitly regulates cutoff frequencies to ensure spectral compatibility with downstream processing workflows, including terrain correction. Flight experiments demonstrate that the K-F method achieves a repeat-line internal consistency of 0.558 mGal at 0.01 Hz-a 65.3% accuracy improvement over standalone FIR filtering (1.606 mGal at 0.01 Hz). Concurrently, it enhances spatial resolution to 2.5 km (half-wavelength), enabling the recovery of data segments corrupted by airflow disturbances that were previously unusable. Implemented on the GIPS-1A system, K-F enables precision mineral exploration and establishes a noise-suppressed paradigm for extreme-dynamic gravimetry.

Keywords: airborne gravity; finite impulse response filter; Kalman filter; fusion filter



Academic Editors: Paulo T.L. Menezes and Valeria Barbosa

Received: 23 June 2025 Revised: 4 August 2025 Accepted: 7 August 2025 Published: 26 August 2025

Citation: Wang, G.; Xiong, S.; Yan, F.; Luo, F.; Wang, L.; Zhou, X. Kalman–FIR Fusion Filtering for High-Dynamic Airborne Gravimetry: Implementation and Noise Suppression on the GIPS-1A System. *Appl. Sci.* **2025**, *15*, 9363. https://doi.org/10.3390/app15179363

Copyright: © 2025 by the authors. Licensee MDPI, Basel, Switzerland. This article is an open access article distributed under the terms and conditions of the Creative Commons Attribution (CC BY) license (https://creativecommons.org/licenses/by/4.0/).

# 1. Introduction

Airborne gravimetry, as a pivotal technology for efficient and environmentally sustainable acquisition of Earth's gravity field, has been extensively deployed in challenging terrains (e.g., mountains, swamps, and oceans) inaccessible to ground surveys or requiring rapid reconnaissance. It plays a vital role in mineral resource exploration and geological structure research, and related domains [1]. This technique employs aircraft or unmanned aerial vehicles (UAVs) as platforms, integrating dual-channel measurements from airborne gravimeters and differential GNSS (Global Navigation Satellite System). During survey flights, the output signal of the gravimeter's vertical sensor contains composite information

comprising true gravitational acceleration, motion-induced acceleration, and multi-source noise. The core objective of airborne gravity data processing is to extract gravity anomalies from this composite signal. However, the acquired gravity data exhibit severely degraded signal-to-noise ratios (SNR  $< 10^{-5}$ – $10^{-6}$ ) due to multi-source interference, including airflow disturbances (e.g., wind shear, wingtip vortices), platform vibrations, and sensor noise [2]. Consequently, achieving effective noise suppression while preserving the spectral integrity of weak gravity anomalies remains a critical challenge for improving measurement accuracy.

Widely adopted approaches include low-pass filtering [3–5] and Kalman filtering [6–12]. The finite impulse response (FIR) filter is widely utilized in airborne gravimetric data processing due to its deterministic frequency-domain selectivity. By optimizing its design parameters, the FIR filter effectively suppresses high-frequency interference components while retaining the primary gravity signal content. However, despite the predominant spectral concentration of gravity anomalies within targeted bands, the absence of a distinct transition between signal and noise spectra limits the efficacy of conventional FIR implementations. Static filter configurations fail to adapt to the time-varying noise profiles inherent to airborne platforms, resulting in incomplete suppression of non-stationary disturbances and insufficient separation of spectrally overlapping signal–noise mixtures. In contrast, Kalman filtering (a recursive time-domain estimation method) excels in dynamic environments by constructing state-space models to decouple gravity anomalies from noise, with demonstrated efficacy in mitigating platform-induced disturbances [6]. Nevertheless, its lack of explicit frequency-domain control hinders compatibility with downstream geophysical workflows (e.g., terrain correction requiring frequency-matched filtering), thereby limiting its engineering adoption.

To synergize the complementary strengths of FIR and Kalman filters, Zou et al. [13] proposed a cascaded filtering framework for strapdown airborne gravimeters. Their method sequentially applies Kalman filtering and FIR low-pass filtering (fc = 0.00625 Hz) to raw gravity data, achieving a 17.2% improvement in repeat-line internal consistency accuracy (1.2 mGal vs. 1.45 mGal for standalone FIR). While innovative, their Markov-model-based state-space formulation assumes stationary noise statistics, rendering it ineffective against time-varying interference spectra encountered in actual flights. Despite its conceptual merit, the achieved precision (1.2 mGal) remains insufficient for operational requirements. Alternative methods, such as wavelet transform [14], improved function filter [15], and minimum curvature techniques [16], have also been explored but face limitations in dynamic adaptability or computational practicality, preventing widespread application. For a comprehensive methodological comparison, see Table 1. Addressing these limitations, this study introduces a novel Kalman-FIR fusion filtering (K-F) algorithm tailored for airborne gravimetry systems. The K-F framework combines adaptive Kalman filtering for dynamic noise suppression with deterministic FIR post-filtering to enforce explicit spectral constraints. Validated through flight tests on the GIPS-1A airborne gravimeter, the method demonstrates dual capabilities: preserving Kalman's noise suppression robustness in dynamic environments and providing FIR's frequency-domain transparency. Operational deployment on the GIPS-1A system has enabled high-precision gravity surveys in complex terrains, establishing a practical engineering solution that harmonizes noise attenuation and spectral fidelity.

In airborne gravity measurements, gravity anomaly signals are intrinsically coupled with aircraft motion-induced accelerations. When the platform encounters in-flight disturbances (e.g., turbulence, maneuvers), horizontal accelerations become partially coupled into the gravimeter's vertical sensor, significantly degrading measurement accuracy. Existing studies generally lack separate consideration for such interference induced by horizontal

Appl. Sci. 2025, 15, 9363 3 of 17

motion coupling, primarily relying on increasing the filtering bandwidth of vertical signals to suppress such interference. This approach compromises the half-wavelength spatial resolution and attenuates genuine gravity anomaly information. This persistent limitation stems from a disconnect between instrument developers and operational end-users: developers often overlook application-specific interference profiles, while operators rarely delve into underlying instrument technologies.

**Table 1.** Comparison of airborne gravity data processing methods.

Algorithm	Core Principle	Physical Significance and Characteristics for Gravity Anomaly Extraction	Engineering Application Status
FIR filtering [3]	Digital filter design	<ul> <li>Clear spatial resolution</li> <li>Poor dynamic adaptability</li> <li>Resolution-accuracy tradeoff under disturbances</li> </ul>	<ul> <li>Longest-developed and most widely applied method</li> <li>Achieves up to 3 km half-wavelength resolution in stable flights</li> </ul>
Kalman filtering [9]	State-space estimation	<ul> <li>Unclear spatial resolution</li> <li>Moderate dynamic adaptability</li> <li>Focused on vertical sensor signals</li> </ul>	<ul> <li>Rapidly developed in recent decades</li> <li>Controversial in industrial applications</li> <li>Primarily used for FIR result verification</li> </ul>
Wavelet transform [14]	Time-frequency multiscale decomposition	<ul><li>Unclear spatial resolution</li><li>Suitable for stable flight operations</li></ul>	<ul><li>Theoretically innovative</li><li>Limited practical value</li><li>No widespread adoption</li></ul>
Improved function filter [15]	Digital filter design, controlling the cutoff frequency and transition band length of the filter	<ul><li>Clear spatial resolution</li><li>Suitable for stable flight operations</li></ul>	<ul> <li>Theoretically innovative</li> <li>Limited practical value</li> <li>No widespread adoption</li> <li>Achieves 3.5 km half-wavelength resolution</li> </ul>
Minimum curvature techniques [16]	Surface interpolation fitting	<ul><li>Unclear spatial resolution</li><li>Suitable for stable flight operations</li></ul>	<ul><li>Theoretically innovative</li><li>Limited practical value</li><li>No widespread adoption</li></ul>
Kalman–FIR fusion filtering	Digital filter design and state-space estimation	<ul> <li>Explicit spatial resolution</li> <li>Maximizes retention of broadband information</li> <li>Balances resolution and high accuracy</li> <li>Integrates vertical and horizontal sensor data</li> <li>Superior dynamic adaptability</li> </ul>	<ul> <li>Equipped with GIPS-1A gravimeter</li> <li>Widely deployed in marine and high-altitude engineering operations</li> <li>Achieves up to 2.5 km half-wavelength resolution in high dynamic flight</li> </ul>

Based on an in-depth understanding of the design and measurement principles of platform-type airborne gravimeters, this study fully utilizes the unique attitude isolation and stability maintenance capabilities of platform gravimeters. For the first time, it systematically constructs and incorporates a horizontal motion coupling interference error model,

Appl. Sci. 2025, 15, 9363 4 of 17

achieving effective estimation and compensation for interference signals introduced by motion accelerations in both horizontal directions.

The innovative contributions of this study in airborne gravity data processing and its engineering applications are summarized as follows:

- (1) Based on the working principles and hardware characteristics of platform-type triaxial gravimeters, short-term platform misalignment angle linearized state equations are established. This model introduces horizontal motion acceleration information into the gravity anomaly estimation state equation, expanding the state space of existing Kalman filtering methods to directly compensate for horizontal motion interference. This state estimation equation effectively improves gravity measurement accuracy in high-dynamic flight regions without sacrificing half-wavelength resolution.
- (2) A deterministic finite impulse response (FIR) filter is cascaded to form the innovative Kalman–FIR fusion (K-F) framework. This design ensures clear mapping of physical meaning (spatial resolution) in gravity anomaly data processing; explicit spectral control guarantees compatibility with downstream processes like terrain correction, while eliminating application barriers caused by spectral opacity of Kalman filtering.

# 2. Methodology

The extraction of airborne gravity anomalies comprises three sequential steps: multisource data synchronization, comprehensive gravity corrections, and noise elimination. The procedural workflow is illustrated in Figure 1. Specifically, it includes the following steps:

- (1) Unify sampling rates and synchronize time signals between the gravity sensor channel data and differential satellite navigation data.
- (2) Apply corrections:
  - Gravity sensor data: Zero-drift correction and reference point calibration;
  - Differential satellite data: Eccentricity correction, Eötvös correction, and normal field correction;
  - Integrate all corrected results to generate the raw gravity anomaly.
- (3) Filter the raw anomaly to extract the gravity anomaly signal.

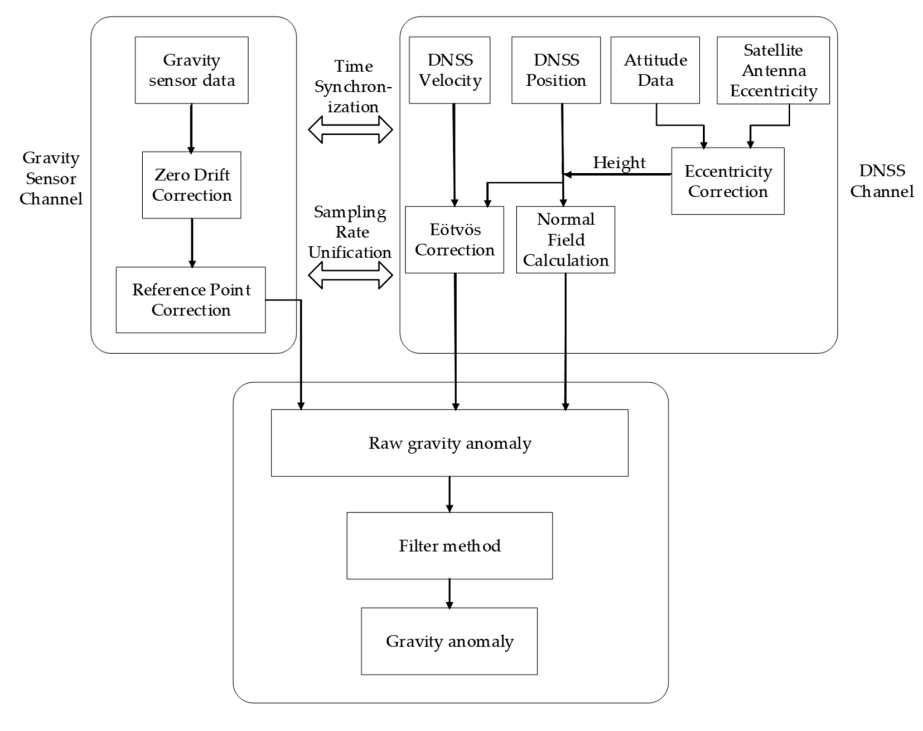


Figure 1. Flowchart of gravity anomaly extraction.

Appl. Sci. **2025**, 15, 9363 5 of 17

# 2.1. Data Synchronization

Airborne gravimetry comprises two parallel measurement systems: (1) Differential satellite data measurement acquires the gravimeter's velocity and position; (2) gravimeter sensors measure triaxial accelerations (east, north, vertical) and attitude data. For the GIPS-1A system, the gravimeter outputs data at 100 Hz while differential GNSS provides data at 2 Hz. Adhering to the Nyquist sampling theorem, this study downsampled the gravimeter outputs and performed temporal alignment using timestamp interpolation.

## 2.2. Comprehensive Gravity Corrections

The idealized measurement model assumes a perfectly leveled instrument platform:

$$\Delta g = f_u - \dot{v}_u + \Delta G_E - G(\varphi, h) \tag{1}$$

where

 $\Delta$ g: Gravity anomaly;

 $f_u$ : Observed gravity under platform-leveled conditions;

 $\Delta G_E$ : Eötvös correction;

 $G(\varphi, h)$ : Normal gravity at the computation point.

Actual flight dynamics induce platform tilting, requiring revision to

$$\Delta g = f_z - \dot{v}_u + \Delta G_E - G(\varphi, h) \tag{2}$$

where  $f_z$  denotes the vertical component of  $f_u$  (true sensor measurement).

As airborne gravimetry constitutes relative measurement, pre-flight static observations at airport base stations establish datum ties:

$$\Delta g = g_b + (f_z - f_{z0}) - \dot{v}_u + \Delta G_E - G(\varphi, h) + \delta a_K + \delta a_I \tag{3}$$

where  $g_b$  is the reference gravity at the airport,  $f_z$  and  $f_{z0}$  denote the observed vertical gravity component and its initial value,  $\delta a_K$  represents the zero-drift correction, and  $\delta a_I$  encompasses random noise from both the gravimeter and differential GNSS.

# 2.3. FIR Low-Pass Filtering

The FIR filter is an all-zero system with guaranteed stability and straightforward design. The output signal y(n) of an N-th order FIR filter can be expressed as the convolution of the input signal x(n) and the filter's impulse response h(k):

$$y(n) = \sum_{k=0}^{N-1} h(k)x(n-k)$$
 (4)

where h(k) denotes the filter coefficients.

To approximate the infinite impulse response of an ideal filter, FIR design employs finite-length window functions w(n) to truncate the primary components of  $h_d(n)$ :

$$h(n) = h_d(n).\omega(n), n = 0, 1, 2, \dots, N - 1$$
 (5)

Common window functions include the Hanning, Hamming, and Blackman windows. Among these, the Hanning window is frequently regarded as better suited to the extraction

Appl. Sci. **2025**, 15, 9363 6 of 17

of airborne gravity anomalies; therefore, this study employs the Hanning window as the window function. Its mathematical form is as follows:

$$\omega(n) = \begin{cases} \frac{1}{2} \left( 1 - \cos \frac{2\pi n}{N-1} \right), 0 \le n \le N-1 \\ 0, n \text{ are others} \end{cases}$$
 (6)

# 2.4. Kalman Filtering

Unlike frequency-domain filtering methods that treat noise as undesirable signals to be removed, the Kalman filter leverages statistical properties of system noise and measurement noise to estimate useful signals—fundamentally representing an optimal estimation theory known as recursive minimum linear variance estimation. As a time-domain filtering technique applicable to multidimensional and non-stationary stochastic processes, the Kalman filter operates as follows:

Let the system state  $X_k$  at time k be driven by system noise  $W_k$  and deterministic inputs  $U_k$ . The state-space representation is

$$\mathbf{X}_{k+1} = \mathbf{\Phi}_k \mathbf{X}_k + \mathbf{B}_k \mathbf{U}_k + \mathbf{\Gamma}_k \mathbf{W}_k \tag{7}$$

$$\mathbf{Z}_k = \mathbf{H}_k \mathbf{X}_k + \mathbf{V}_k \tag{8}$$

where

 $\Phi_k$ ,  $H_k$ : State transition and measurement matrices;

 $\mathbf{B}_k$ : Control input matrix;

 $\Gamma_k$ : System noise driving matrix;

 $W_k$ ,  $V_k$ : Zero-mean white noise with covariances  $Q_k$  and  $R_k$ , respectively, satisfying

$$E[\mathbf{W}_k \mathbf{W}_i^T] = \mathbf{Q}_k \delta_{kj}, E[\mathbf{V}_k \mathbf{V}_i^T] = \mathbf{R}_k \delta_{kj}$$
(9)

Here,  $\mathbf{Q}_k$  is non-negative definite, and  $\mathbf{R}_k$  is positive definite [17].

The discrete fundamental equations of Kalman filtering (10)–(14) enable recursive solutions to both the state (7) and measurement Equation (8).

State One-Step Prediction:

$$\mathbf{X}_{k,k-1} = \mathbf{\Phi}_{k-1} \mathbf{X}_{k-1} + \mathbf{B}_{k-1} \mathbf{U}_{k-1} \tag{10}$$

State Estimation:

$$\mathbf{X}_k = \mathbf{X}_{k,k-1} + \mathbf{K}_k(\mathbf{Z}_k - \mathbf{H}_k \mathbf{X}_{k,k-1}) \tag{11}$$

Filter Gain:

$$\mathbf{K}_{k} = \mathbf{P}_{k,k-1} \mathbf{H}_{k}^{T} (\mathbf{H}_{k} \mathbf{P}_{k,k-1} \mathbf{H}_{k}^{T} + \mathbf{R}_{k})^{-1}$$

$$(12)$$

One-Step Prediction Mean Square Error:

$$\mathbf{P}_{k,k-1} = \mathbf{\Phi}_{k-1} \mathbf{P}_{k-1} \mathbf{\Phi}_{k,k-1}^T + \mathbf{\Gamma} \mathbf{Q} \mathbf{\Gamma}^T$$
 (13)

Estimated Mean Square Error:

$$\mathbf{P}_{k} = (\mathbf{I} - \mathbf{K}_{k} \mathbf{H}_{k}) \mathbf{P}_{k,k-1} (\mathbf{I} - \mathbf{K}_{k} \mathbf{H}_{k})^{T} + \mathbf{K}_{k} \mathbf{R}_{k} \mathbf{K}_{k}^{T}$$
(14)

Appl. Sci. 2025, 15, 9363 7 of 17

## 2.5. Kalman–FIR Fusion Filtering (K-F Filtering)

In airborne gravimetric practice, the mathematical model for gravity anomalies is formulated based on Newton's second law by analyzing the forces acting on the measurement platform and its flight dynamics:

$$\Delta g = f_{\Sigma} - \dot{v}_{u} + q_{\Sigma} \tag{15}$$

where

 $\Delta g$ : Gravity anomaly;

 $f_{\Sigma}$ : Corrected gravity value incorporating normal field, elevation, Eötvös, drift, and base station corrections;

 $\dot{v}_u$ : Vertical acceleration of the aircraft;

 $q_{\Sigma}$ : Aggregate noise from multi-source disturbances.

Notably,  $f_{\Sigma}$  and  $\dot{v}_u$  can be derived from differential GNSS signals and raw gravimetric measurements. Their computational methodologies are beyond the scope of this paper and are treated as known quantities [18].

To enable dynamic compensation of airborne gravity anomalies, the aggregate error  $q_{\Sigma}$  is decomposed into four components: (1) X-axis gravitational-acceleration-induced error; (2) Y-axis gravitational-acceleration-induced error; (3) Z-axis gravitational-acceleration-induced error; (4) residual noise.

Three calibration coefficients  $(S_x, S_y, S_z)$  are introduced into the gravity anomaly model to independently regulate errors caused by gravitational accelerations  $(f_x, f_y, f_z)$  along each axis:

$$\Delta g = f_{\Sigma} - \dot{v}_u + S_x f_x + S_y f_y + S_z f_z + q_{others}$$
(16)

It is noteworthy that the effective operation and optimal estimation performance of Equation (16) critically depend on one prerequisite: the inertial stabilized platform must maintain real-time attitude tracking and stabilization capability. Under this condition,  $S_x$  and  $S_y$  physically represent the platform misalignment angles over short time intervals.

Furthermore, within short time scales,  $S_x$  and  $S_y$  are predominantly attributed to the null drift of horizontal-axis gyroscopes in the gravimeter. Given the minute magnitude of these angles, they can be linearized as first-order constants, with their time derivatives quantitatively characterizing the gyroscopic drift rate.

Equation (7) is rewritten into a Kalman filter state-space representation:

$$\dot{h} = v_{u}$$

$$\dot{v}_{u} = f_{\Sigma} + S_{x}f_{x} + S_{y}f_{y} + S_{z}f_{z} - \Delta g + q_{others}$$

$$\dot{S}_{x} = q_{S_{x}}$$

$$\dot{S}_{y} = q_{S_{y}}$$

$$\dot{S}_{z} = q_{S_{z}}$$

$$h' = H_{f}X_{f} + \delta h$$
(17)

where

h': Measured reference ellipsoid height;

 $\delta$  h: Measurement error of h'.

The parameterization adopts

$$\mathbf{X}_f = \begin{pmatrix} h & v_u & S_z & S_y & S_x \end{pmatrix}^T$$
,  $\mathbf{H}_f = \begin{pmatrix} 1 & 0 & 0 & 0 & 0 \end{pmatrix}^T$ 

Appl. Sci. 2025, 15, 9363 8 of 17

The gravity anomaly is modeled as a random process using a forming filter:

$$\dot{\mathbf{X}}_{g} = \mathbf{A}_{g}\mathbf{X}_{g} + \mathbf{\Gamma}_{g}\mathbf{q}_{g} 
\Delta g = \mathbf{H}_{g}\mathbf{X}_{g}$$
(18)

where

 $X_g$ : State vector to be estimated;

 $A_g$ ,  $\Gamma_g$ : Constant system matrices;

 $\mathbf{q}_g$ : White noise with intensity  $\mathbf{Q}_g$ .

The parameterization adopts

$$\mathbf{X}_g = \begin{pmatrix} \Delta g \\ \Delta \dot{g} \end{pmatrix}$$
,  $\mathbf{A}_g = \begin{pmatrix} 0 & 1 \\ 0 & 0 \end{pmatrix}$ ,  $\mathbf{\Gamma}_g = \begin{pmatrix} 0 \\ 1 \end{pmatrix}$ ,  $\mathbf{H}_g = \begin{pmatrix} 1 & 0 \end{pmatrix}$ .

By combining Equations (17) and (18), the unified state-space model is derived.

To synergize the dynamic adaptation capability of Kalman filtering with the well-defined cutoff frequency of FIR low-pass filtering, the proposed K-F algorithm operates as follows:

# (1) Kalman Filtering Stage:

Estimate the calibration coefficients ( $S_x$ ,  $S_y$ ,  $S_z$ ) via Kalman filtering to dynamically adjust axis-specific errors.

# (2) Error Compensation:

Subtract the calibrated errors  $(S_x, S_y, S_z)$  from the corrected gravity field  $f_{\Sigma}$  using Equation (7), yielding a noise-contaminated gravity anomaly  $\Delta g_{noisy}$ .

$$\Delta g_{noisy} = f_{\Sigma} - \dot{v}_u - (S_x f_x + S_y f_y + S_z f_z) \tag{19}$$

# (3) FIR Post-Filtering:

Apply a low-pass FIR filter with a predefined cutoff frequency  $f_c$  to suppress residual noise in  $\Delta g_{noisy}$ , producing the refined gravity anomaly  $\Delta g$  final.

$$\Delta g_{final} = \text{FIR}(\Delta g_{noisy}, f_c)$$
 (20)

The workflow is illustrated in Figure 2.

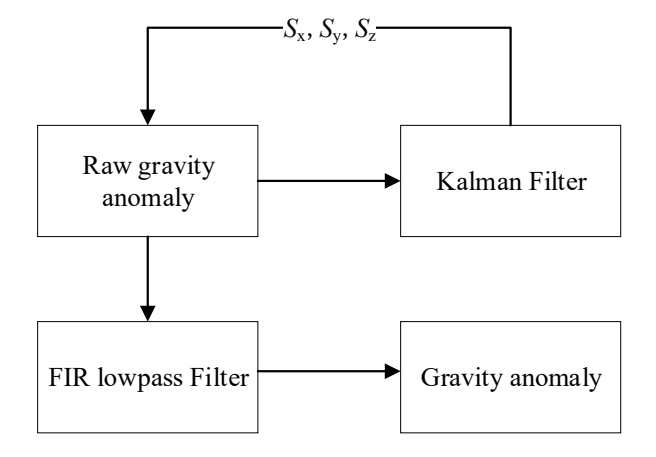


Figure 2. Flowchart of K-F filtering algorithm.

Appl. Sci. 2025, 15, 9363 9 of 17

## 2.6. Quality Evaluation Method

The internal consistency accuracy of airborne gravimetry is evaluated using repeat-line test data to assess the dynamic precision of repeated measurements. This metric quantifies the agreement between multiple repeat-line datasets relative to their averaged gravity field, reflecting the system's dynamic performance [19,20].

For each repeat line, the root mean square internal consistency accuracy is calculated as

$$\sigma_j = \sqrt{\frac{\sum_{i=1}^n \left(\Delta g_{ij} - \overline{\Delta g_i}\right)^2}{n}}, (j = 1, 2, \dots, m)$$
(21)

 $\Delta g_{ij}$ : Gravity anomaly at point i on repeat line j;

 $\overline{\Delta g_i} = \frac{1}{m} \sum_{i=1}^{m} \Delta g_{ij}$ : Mean gravity anomaly at point *i* across all repeat lines;

*m*: Number of repeat lines;

n: Number of data points in the common segment of repeat lines.

The overall internal consistency accuracy across all repeat lines is given by

$$\sigma_j = \sqrt{\frac{\sum\limits_{j=1}^{m}\sum\limits_{i=1}^{n} \left(\Delta g_{ij} - \overline{\Delta g_i}\right)^2}{m \times n}}$$
 (22)

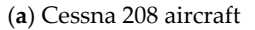
# 3. Field Data Validation

### 3.1. Survey Overview

This study validates the K-F filtering using actual measurement data. The test employed the GIPS-1A platform-type airborne gravimeter, jointly developed by China Aero Geophysical Survey & Remote Sensing Center and Beijing Institute of Automation Control Equipment, implementing a "three-axis stabilized platform + quartz-flexure accelerometer" design.

The test was conducted aboard a Cessna 208B (Figure 3) fixed-wing aircraft over a maritime survey line (Line 2010, ~60 km north–south trending, GPS altitude: 600 m, ground speed: 220 km/h). Due to airspace and weather constraints, the measurements were conducted at midday when airflow disturbances were more complex compared to other periods.







(b) GIPS-A gravimeter

Figure 3. Installation of the GIPS-A gravimeter in an amphibious Cessna 208 aircraft.

The flight path is illustrated in Figure 4. The aircraft took off from the airport, reached the survey area, and executed two round-trip flights along the east–west survey lines, resulting in four repeated east–west survey lines (two pairs). A single north–south round-

trip flight was also conducted, yielding a pair of repeated north–south survey lines. Due to the limited number of north–south lines, statistical analysis was only performed on the east–west lines. For these four repeated east–west lines, raw gravity anomalies ranged from -31,715.506 to 27,754.607 mGal and showed an internal consistency accuracy of 4349.245 mGal (Figure 5). This indicates complete signal masking by noise and an absence of repeat-line coherence.

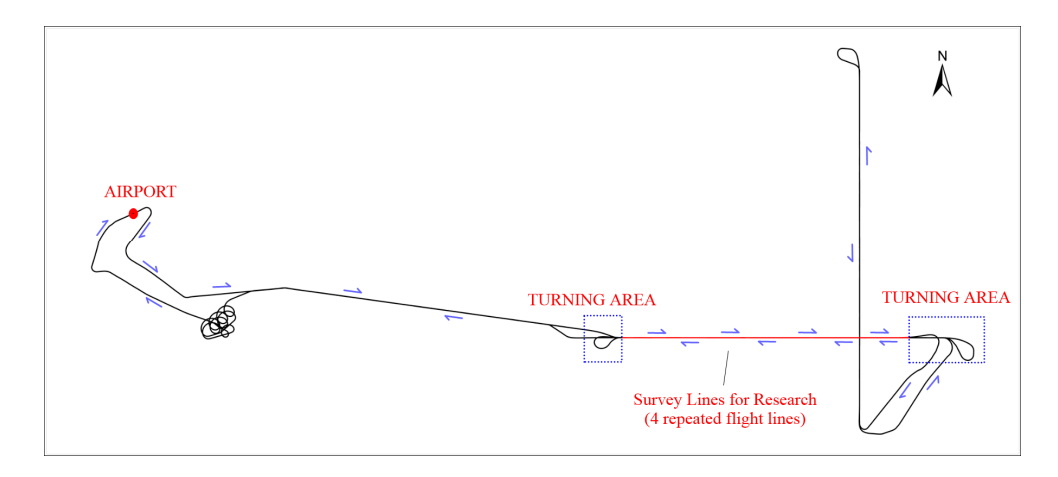


Figure 4. Test flight track map.

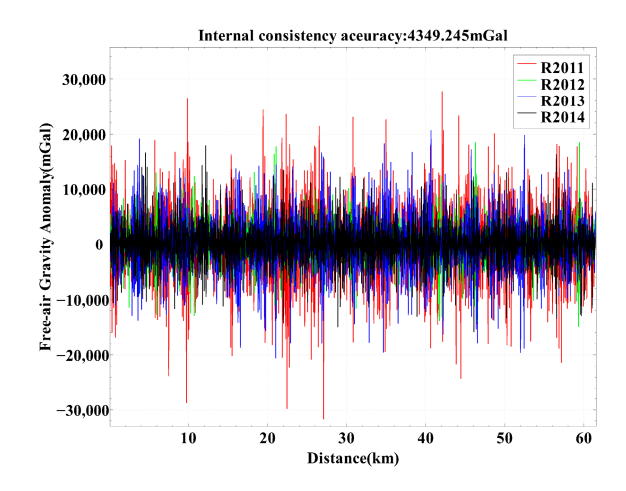


Figure 5. Raw gravity anomaly map K-F filtering algorithm flowchart.

# 3.2. Repeated Line Data Processing Results

In airborne gravity surveys, the determination of filtering parameters and geospatial half-wavelength resolution adheres to stringent physical constraints: the cutoff frequency  $(f_c)$  of low-pass filtering or time window length (T filter) combined with flight velocity (T0) dictates the minimum resolvable half-wavelength (T1) for geological structures. While the selection of filtering parameters and their impact on resolution are relatively straightforward, the core challenge lies in balancing high-frequency noise suppression (e.g., >10 mGal spikes induced by airflow disturbances) and short-wavelength signal preservation (essential for resolving geological features like faults or salt dome boundaries).

In operational airborne engineering applications, a 100 s low-pass filter (cutoff frequency:  $0.01~\rm Hz$ ) is typically applied, with an internal consistency accuracy threshold of  $0.8~\rm mGal$  deemed acceptable for production-grade data (half-wavelength spatial resolution: ~3 km) [20]. For comparative analysis, both FIR and K-F filters were tested at three cutoff settings:  $80~\rm s$  ( $0.0125~\rm Hz$ ),  $100~\rm s$  ( $0.01~\rm Hz$ ), and  $120~\rm s$  ( $0.00833~\rm Hz$ ). The gravity anomaly along the line exhibits an inverted "S" morphology with amplitudes of 50–60 mGal, transitioning

smoothly to background values at the edges. Results are summarized in Figures 6–8 and Table 2.

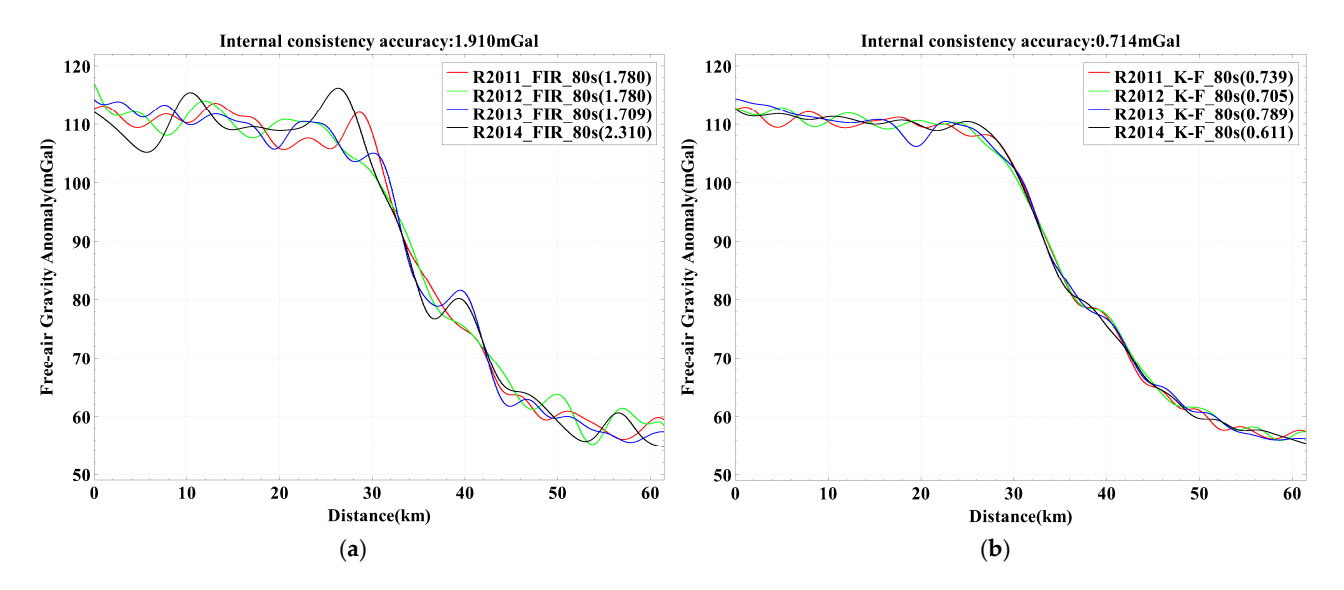


Figure 6. Processing results of FIR (a) and K-F filter (b) with 80 s filtering time.

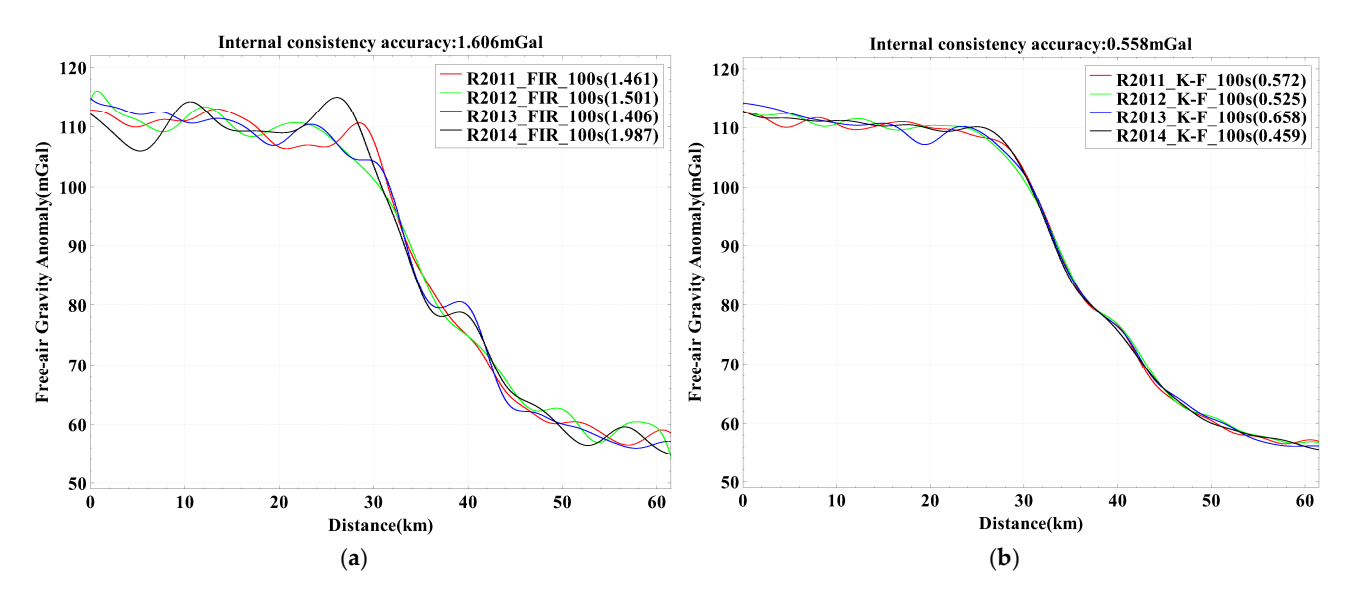


Figure 7. Processing results of FIR (a) and K-F filter (b) with 100 s filtering time.

Table 2. Comparison of processing results of FIR Filter and K-F Filter.

Filter Time (s)	Half-Wavelength (km)	FIR Filter (mGal)	K-F Filter (mGal)	Improvement Percentage
80	2.44	1.910	0.714	62.62%
100	3.06	1.606	0.558	65.26%
120	3.67	1.414	0.475	66.41%

Table 2 shows that the FIR-filtered data exhibited internal consistency accuracies of 1.910 mGal (80 s), 1.606 mGal (100 s), and 1.414 mGal (120 s), with persistent artifacts and false anomalies attributed to low-frequency airflow-disturbance-induced noise unattenuated by conventional filtering. Extending the filtering window to 120 s marginally improved repeatability but degraded spatial resolution (half-wavelength > 3 km), rendering the dataset operationally unusable. In contrast, the K-F algorithm achieved significantly higher precision, with internal consistency accuracies of 0.714 mGal (80 s), 0.558 mGal

(100 s), and 0.475 mGal (120 s), corresponding to improvements of 62.6%, 65.3%, and 66.4% over FIR filtering, respectively. The K-F framework demonstrated superior airflow disturbance resistance, suppressing low-frequency noise while preserving spectral integrity and achieving a half-wavelength spatial resolution of ~2.5 km.

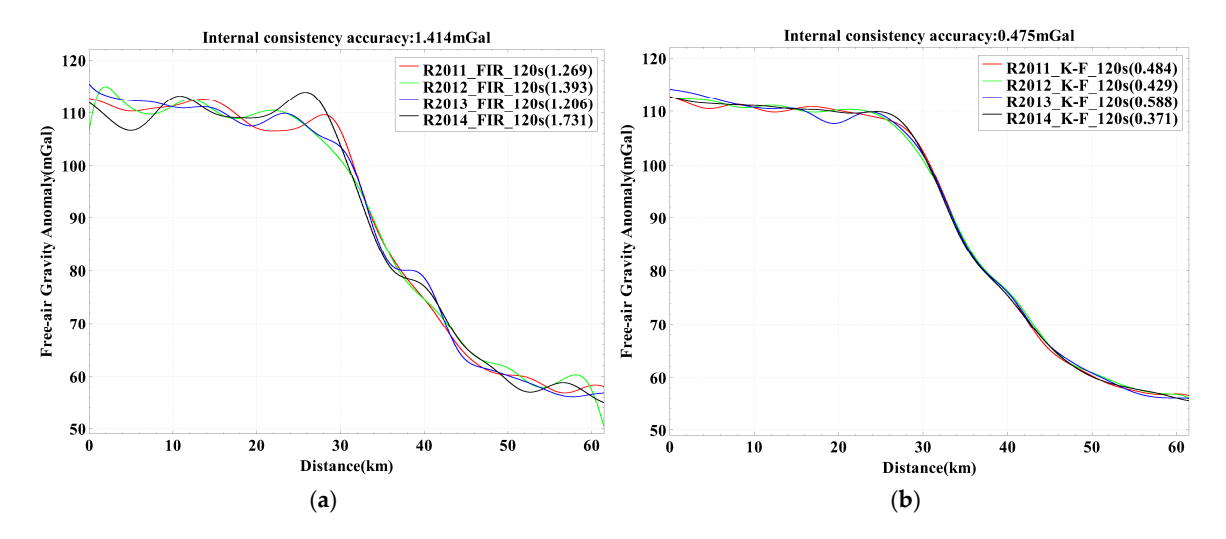


Figure 8. Processing results of FIR (a) and K-F filter (b) with 120 s filtering time.

This validation confirms the K-F algorithm's engineering viability for high-dynamic airborne gravimetry, particularly in challenging survey environments. It should be emphasized that while the K-F filter demonstrated a significant improvement in data processing results compared to the FIR filter in this particular experiment, this advantage is not consistently substantial across all flight tests. When the aircraft is in steady-state flight, the processing results achieved by the K-F filter and the FIR filter show comparable performance.

Figure 9 presents the gravity anomaly extraction results from another flight pass, indicating that the FIR filter achieves an internal coincidence accuracy of 0.603~mGal/100~s, while the K-F filter attains 0.564~mGal/100~s. This confirms that the FIR filter can also deliver satisfactory results under steady flight conditions. However, the K-F filter demonstrates superior stability in more complex flight conditions.

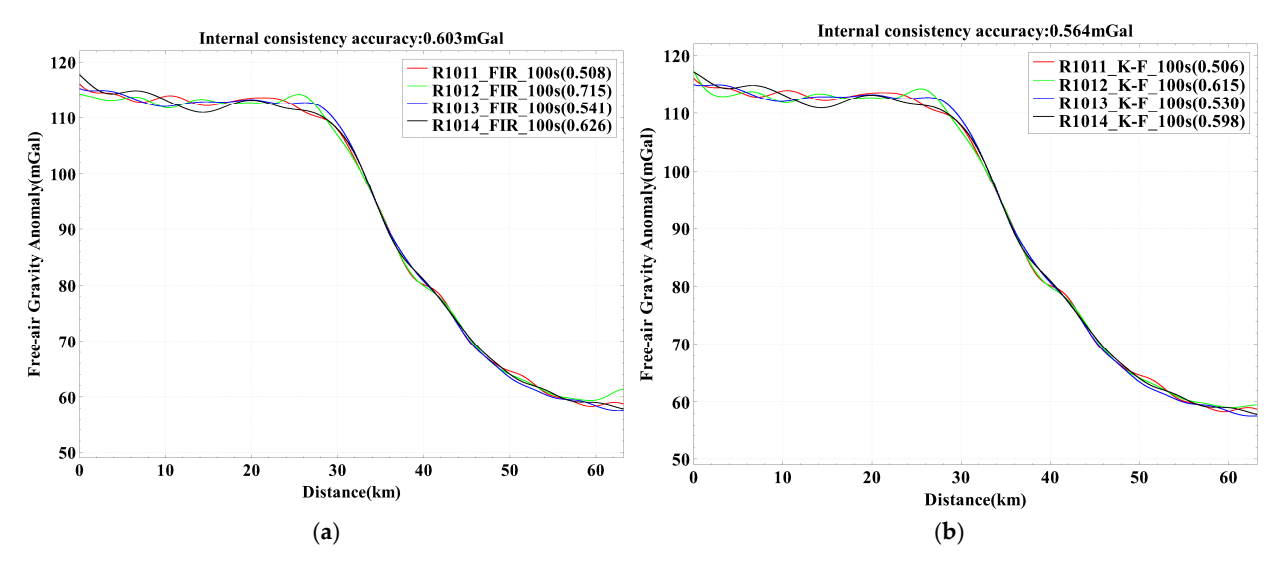


Figure 9. Processing results of FIR (a) and K-F filter (b) with 100 s filtering time.

## 3.3. Full Fight Data Processing Results

To further evaluate the suppression capability of the algorithm against flight platform motion interference, the entire flight sortie data was analyzed using 100 s filtering results as an example. Figure 10 compares the processing results of three methods: K-F filter, FIR filter, and Kalman filter. The repeat-line measurement areas and turning areas are color-coded in cyan and gray, respectively. Considering that gravity anomaly signals inherently exhibit low-frequency slow variations whose theoretical waveforms should not show drastic fluctuations, while the curves in turning areas display large fluctuations, the abnormal oscillations in the figure can be attributed to motion-induced interference from the platform. By measuring the fluctuation amplitude of these curves, the algorithm's motion interference compensation capability can be characterized.

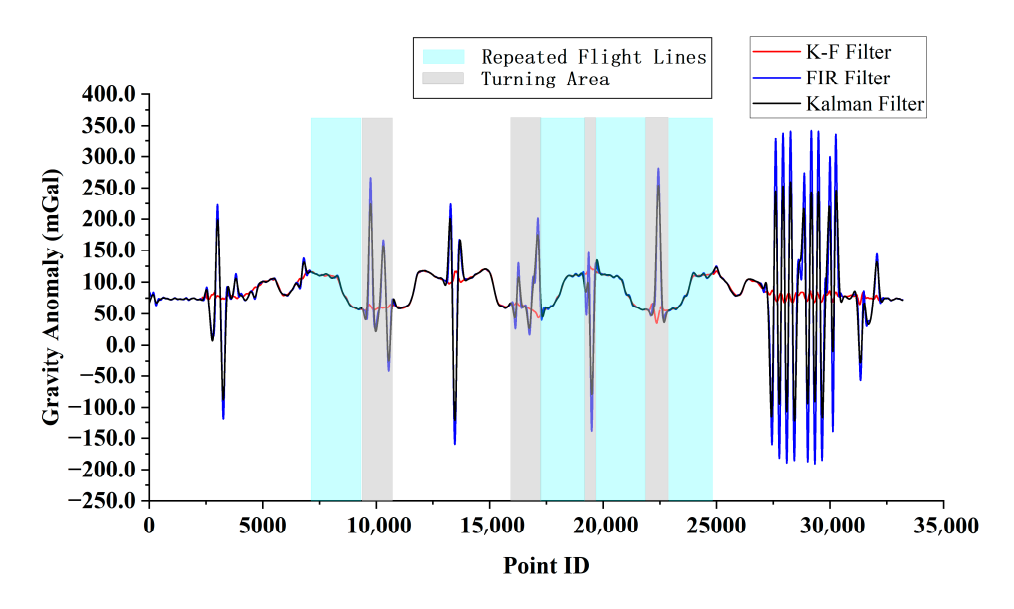


Figure 10. Comparison of processing results: K-F filter vs. FIR filter vs. Kalman filter.

In turning segments (gray zones in Figure 10), fluctuations in the filtered curve of the K-F filter proposed in this paper decreased substantially compared to the other two methods. Statistical results in Table 3 further corroborate this: the K-F filtered output exhibits a peak-to-peak value of only 89.792 mGal (standard deviation: 19.928 mGal), significantly below the FIR filter's peak-to-peak value of 533.342 mGal (standard deviation: 63.036 mGal) and the Kalman filter's peak-to-peak value of 381.775 mGal (standard deviation: 50.390 mGal). Statistical analysis demonstrates that the K-F filter improves motion interference suppression by approximately 5.9 times (vs. FIR) and 4.3 times (vs. Kalman). Figure 11 shows the difference between the K-F filter and FIR filter results, providing a more intuitive visualization of the K-F filter's superior noise attenuation capability compared to the FIR filter.

**Table 3.** Statistical results of flight sortie data processed by three methods.

	K-F Filter (mGal)	FIR Filter (mGal)	Kalman Filter (mGal)
Maximum Value	124.399	342.779	259.569
Minimum Value	34.607	-190.563	-122.206
Peak-to-Peak Value	89.792	533.342	381.775
Standard Deviation	19.928	63.036	50.390
Maximum Peak in Turning Segments	80.620	342.779	243.214

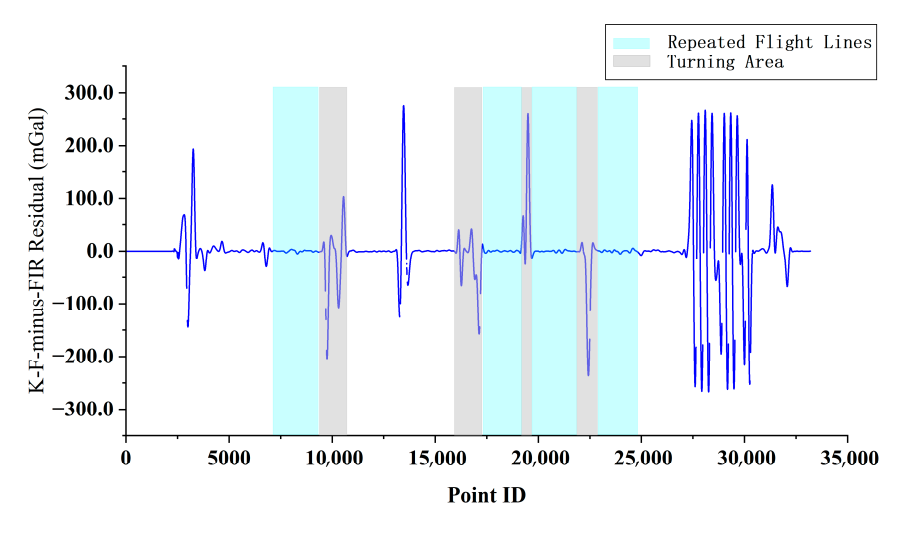
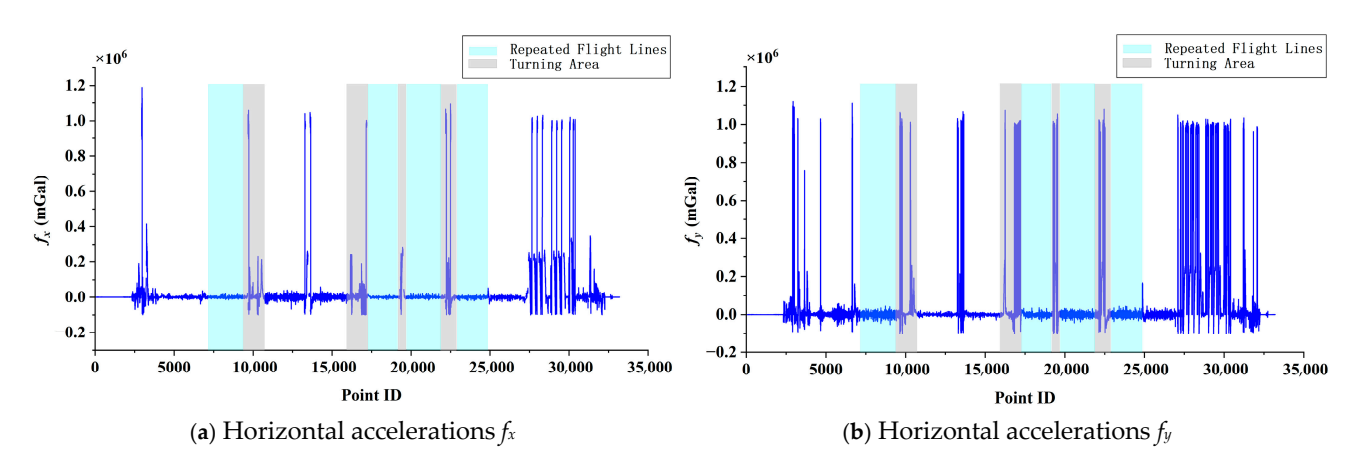
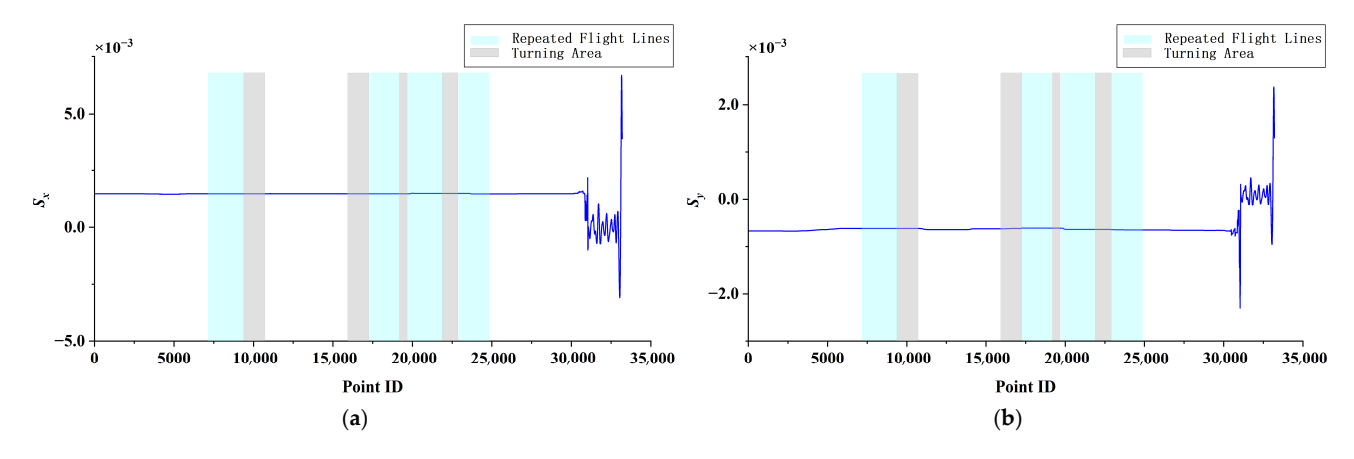


Figure 11. Residual gravity anomaly: K-F filter minus FIR filter.

Figure 12 displays the horizontal motion accelerations  $f_x$  and  $f_y$  during the flight. Values in turning segments exhibit significantly larger magnitudes compared to those during repeat-line flights. Consequently, accurate estimation of platform attitude errors becomes critical for effective horizontal motion interference compensation, specifically the parameters  $S_x$  and  $S_y$  in Equation (12). Figure 13 demonstrates stable convergence of  $S_x$  and  $S_y$  throughout the flight, validating the efficacy of the gravity anomaly estimation state equation.



**Figure 12.** Raw measurements of horizontal accelerations  $f_x$  and  $f_y$ .



**Figure 13.** Processing results of  $S_x$  (**a**) and  $S_y$  (**b**).

# 4. Discussion

To address the challenges of dynamic noise suppression and signal fidelity in airborne gravimetry, this study proposes a novel fusion algorithm integrating Kalman filtering with FIR low-pass filtering (K-F filtering). The algorithm leverages inherent physical design advantages of platform-type gravimeters by linearly representing platform attitude errors and embedding them into the gravity anomaly state estimation equation, thereby compensating for horizontal-motion-induced errors. Additionally, cascaded FIR filters provide explicit cutoff frequency control. Operational validation on the GIPS-1A platform gravimeter confirms the algorithm's efficacy.

# 1. Breakthrough in High-Dynamic Noise Suppression via K-F Filtering

# (1) Enhanced Dynamic Noise Suppression

Through Kalman and FIR filtering, a repeat-line accuracy of 0.558 mGal (65.3% improvement over conventional FIR) is attained on the GIPS-1A system (Figure 6), effectively resolving the conflict between noise contamination from external disturbances and gravimetric signal fidelity. Experimental results demonstrate that under flight conditions of 220 km/h airspeed and airflow disturbances, the K-F algorithm improves repeat-line internal consistency accuracy by over 60% compared to standalone FIR filtering, confirming its robustness against high-dynamic noise.

# (2) Improved Spectral Transparency

Post-Kalman correction, FIR low-pass filtering (80–120 s filtering windows, fc = 0.0083-0.0125 Hz) preserves the dominant low-frequency gravity anomaly band while enabling explicit spectral control to match terrain correction requirements. The achieved half-wavelength spatial resolution of 2.5 km represents a 16.7% improvement over conventional methods (3 km), satisfying the resolution demands for mid- to short-wavelength gravity signals in mineral exploration.

### (3) Extended Engineering Applicability

The constructed joint state-space model quantifies carrier attitude errors by introducing adjustment coefficients ( $S_x$ ,  $S_y$ ,  $S_z$ ), overcoming the stationary state assumption limitation of second-order Markov models. Validation using actual flight mission data demonstrates that this method adapts to noise spectrum variations across different flight missions. Consequently, data previously rendered unusable due to airflow disturbances (FIR filter accuracy: 1.414–1.910 mGal) was recovered to an engineering-applicable level of 0.475–0.714 mGal.

### 2. Foundation for the Efficacy of the K-F Filtering

Gravimeters represent highly complex instrumentation within geological exploration, creating inherent industry barriers. Manufacturers focus predominantly on hardware development with limited insight into field operational scenarios, while exploration entities lack expertise in instrument principles and design details. Consequently, gravity data acquired in complex environments cannot be fully deciphered to isolate inherent interference and noise, diminishing the value of high-cost measurements. Academic institutions primarily engage in theoretical research, collectively sustaining technical disconnects in gravity surveying.

The GIPS-1A platform gravimeter employed in this study possesses geodetic frame stabilization capability through its three-axis inertially stabilized platform. The system adopts a design scheme comprising a "dynamically tuned gyro + resolver + analog control circuit," with all stages processing analog signals exclusively. This configuration delivers strong dynamic response capability, high control bandwidth, and exceptional platform stability, outperforming other platform gravimeters utilizing digital sensing and control solutions.

Under stable flight conditions with only the vertical acceleration channel considered, differences between gravimeters are minimal. However, during high-dynamic flight conditions requiring precise compensation for dual-axis horizontal accelerations, the GIPS-1A gravimeter provides instrument-level physical capability assurance. This constitutes the fundamental prerequisite for linearized modeling of platform attitude errors and their compensation via optimal estimation methods.

# 3. Future Research Perspectives and Recommendations

Building upon the contributions of this work, further research can be advanced through the following two dimensions to refine methodological robustness and theoretical foundations:

(1) Construction of a precise gravimetric measurement model:

The current model's noise identification capability originates from explicit parameterization of platform motion errors  $(S_x, S_y, S_z)$ . Future work must establish a noise–gravity anomaly coupling theory to quantify statistical characteristics of motion interference under varying meteorological conditions (e.g., correlation between kinematic noise power spectrum and Kalman gain  $K_k$ ), providing physical constraints for model parameters.

(2) Enhancement of adaptive anti-disturbance mechanisms:

To further improve robustness against airframe motion disturbances, adaptive noise covariance estimation (real-time updates of  $\mathbf{Q}_k$ ,  $\mathbf{R}_k$ , Equation (9)) can be introduced. This adaptive estimation dynamically responds to non-stationary disturbances during flight, eliminating spectral leakage caused by unmodeled high-frequency interference, thereby maintaining stability of gravity anomaly resolution during abrupt variations in aircraft motion.

# 5. Conclusions

The Kalman–FIR fusion filtering (K-F) method proposed in this study successfully resolves the inherent conflict between noise suppression and signal fidelity in high-dynamic airborne gravimetry through a dual-mechanism approach combining dynamic error compensation and spectral constraints. Its core value manifests in two aspects: (1) The dynamic compensation mechanism overcomes limitations of static filters in adapting to non-stationary noise, maintaining stable system output even in complex meteorological conditions. (2) Explicit spectral control ensures compatibility between gravity anomaly signals and downstream processes like terrain correction, eliminating application barriers caused by the frequency-domain opacity of Kalman filtering.

This achievement marks a technological transition for airborne gravimetry from "single-dimensional noise reduction" to "dynamic-spectral co-optimization". The method has been implemented in the GIPS-1A gravimetry system and deployed across UAVs, helicopters, and fixed-wing aircraft platforms for industrial applications.

**Author Contributions:** Methodology, G.W. and F.Y.; Software, G.W.; Data curation, F.L.; Writing—original draft, G.W.; Writing—review & editing, G.W., F.Y., S.X. and X.Z.; Funding acquisition, L.W. All authors have read and agreed to the published version of the manuscript.

**Funding:** This work was funded by the National Key Research and Development Program of China (Grant No. 2023YFB3907703).

**Institutional Review Board Statement:** Not applicable.

Informed Consent Statement: Not applicable.

**Data Availability Statement:** The datasets presented in this article are not readily available because the project supporting this paper is currently ongoing; the original gravity data are subject to government-mandated confidentiality requirements and cannot be disclosed to the public.

### **Conflicts of Interest:** The authors declare no conflict of interest.

# References

1. Huang, M.T.; Deng, K.L.; Ouyang, Y.Z.; Wu, T.Q.; Zhai, G.J.; Lu, X.P.; Chen, X.; Liu, M.; Wang, X. Research advances in marine-airborne gravity survey and application technology. *Geomat. Inf. Sci. Wuhan Univ.* **2022**, *47*, 1635–1650.

- 2. Bolotin, Y.V.; Doroshin, D.R. Adaptive filtering of airborne gravimetry data using hidden Markov models. *Mosc. Univ. Mech. Bull.* **2011**, *66*, 63–68. [CrossRef]
- 3. Cai, S.K.; Wu, M.P.; Zhang, K.D. A comparison of digital lowpass FIR-filters in airborne gravimetry. *Geophys. Geochem. Explor.* **2010**, *34*, 74–78.
- 4. Lang, J.; Liang, X.; Liu, L.; Wang, G. Research on the Fourier basis pursuit low pass filter for airborne gravity. *Chin. J. Geophys.* **2018**, *61*, 4737–4745.
- 5. Pan, G.; Wang, M.; Cao, J.; Xiong, Z.; Yu, R.; Cai, S. Improving the Horizontal Components Accuracy of Strapdown Airborne Vector Gravimetry by Yaw Continuous Rotation Modulation. *IEEE Trans. Instrum. Meas.* **2021**, *70*, 8503611. [CrossRef]
- 6. Bolotin, Y.V.; Fedorov, A.V. Accuracy analysis of airborne gravimeter calibration using repeated flight paths. *Mosc. Univ. Mech. Bull.* **2008**, *63*, 60–67. [CrossRef]
- 7. Zheng, W.; Zhang, G.B. Application research on adaptive Kalman filtering for airborne gravity anomaly determination. *Chin. J. Geophys.* **2016**, *59*, 1275–1283.
- 8. Vyazmin, V.; Bolotin, Y.V. Two-Dimensional Kalman Filter Approach to Airborne Vector Gravimetry. *J. Geod. Sci.* **2019**, *9*, 87–96. [CrossRef]
- 9. Wang, G.X.; Luo, F.; Zhou, X.H.; Yan, F. Research on Kalman filter method for weak signal extraction of airborne gravity. *Geophys. Geochem. Explor.* **2021**, *45*, 76–83. [CrossRef]
- 10. Cai, T.J.; Fang, K. A New Method for Determining the Gravity Disturbance Vector in Strapdown Airborne Gravimetry. *IEEE Trans. Instrum. Meas.* **2022**, *71*, 9508607. [CrossRef]
- 11. Jensen, T.E. Spatial resolution of airborne gravity estimates in Kalman filtering. J. Geod. Sci. 2022, 12, 185–194. [CrossRef]
- 12. Ke, F.; Cai, T.J. An Algorithm for Strapdown Airborne Gravity Disturbance Vector Measurement Based on High-Precision Navigation and EGM2008. *Sensors* **2024**, *24*, 5899. [CrossRef] [PubMed]
- 13. Zou, X.L.; Cai, S.K.; Wu, M.P. The airborne gravity signal processing based on Kalman and FIR cascade filter. In Proceedings of the IEEE International Conference on Information and Automation, Ningbo, China, 1–3 August 2016; pp. 1996–2000.
- 14. Liu, L.T.; Xu, H.Z. Wavelets in airborne gravimetry. Chin. J. Geophys. 2004, 47, 490–494. [CrossRef]
- 15. Liu, L.; Liang, X.; Lang, J.; Shi, Z.; Yao, Y.; Hu, H.; Sheng, C. Improved function filter and its application in airborne gravimetry. *Acta Geod. Cartogr. Sin.* **2023**, *52*, 706–713. [CrossRef]
- 16. Wang, H.; Xiong, S.Q.; He, T.; WanYin, W. Noise suppression of airborne gravity data with minimum curvature model. *Chin. J. Geophys.* **2024**, *67*, 3959–3972. [CrossRef]
- 17. Kalman, R.E. A new approach to linear filtering and prediction problems. J. Fluids Eng. 1960, 82, 35–45. [CrossRef]
- 18. Forsberg, R.; Olesen, A.V. Airborne gravity field determination. In *Sciences of Geodesy*; Springer: Berlin, Germany, 2010; pp. 83–104.
- 19. Jiang, Z.X.; Zhang, H.; Guo, Z.H. Calculating method of internal coincidence accuracy in airborne gravimetry. *Geophys. Geochem. Explor.* **2010**, *34*, 672–676.
- 20. DZ/T0381-2021; Specification for Airborne Gravity Survey. Ministry of Natural Resources of China: Beijing, China, 2021.

**Disclaimer/Publisher's Note:** The statements, opinions and data contained in all publications are solely those of the individual author(s) and contributor(s) and not of MDPI and/or the editor(s). MDPI and/or the editor(s) disclaim responsibility for any injury to people or property resulting from any ideas, methods, instructions or products referred to in the content.